PHYSICAL REVIEW D VOLUME 16, NUMBER 9 1 NOVEMBER 1977

Systematic study of $\pi^- p$ backward elastic scattering between 1.28 and 3.0 GeV/c

J. Va'Vra,* R. J. Ott,† and J. M. Trischuk
Physics Department, McGill University, Montreal, Canada

T. J. Richards‡
Physics Department, Saint Louis University, St. Louis, Missouri 63103

L. S. Schroeder§
Institute for Atomic Research and Department of Physics, Iowa State University, Ames, Iowa 50010
(Received 28 March 1977)

We have measured the backward differential cross section in $\pi^- p$ elastic scattering at 31 momenta from 1.28 to 3.0 GeV/c. These measurements covered the center-of-mass angular range of 125°–178° corresponding to $-0.570 \lesssim \cos\theta_{\text{c.m.}} \lesssim -0.999$. Considerable structure in the angular distribution is found. We compare these data with data from other experimets and to predictions made by the latest phase-shift solution. We find, in general, good agreement with other data in the few regions of overlap. The fits from the phase-shift solution do not accurately reproduce these data at low momenta below 1.9 GeV/c but give excellent agreement above this momentum.

INTRODUCTION

The backward differential cross section for $\pi^- p$ elastic scattering has been measured at 31 momenta from 1.28 to 3.0 GeV/c. The measurements cover the center-of-mass range in $\cos\theta_{\text{c.m.}}$ from approximately −0.570 to −0.999. In this paper we present the data, discuss their trend, and compare with existing data and phase-shift solutions. In a subsequent publication we will present an analysis of the data via a direct-channel resonance model.

INCIDENT BEAM

The experiment was performed at the Berkeley Bevatron, in a secondary beam produced by a slow extracted proton beam focused onto a copper production target. Secondaries at a production angle of 2.5° were momentum-analyzed at an intermediate focus with a momentum bite of $\Delta p/p \sim \pm 1.25\%$. The beam was then recombined at a final focus onto a liquid hydrogen target. The beam spot size at the final focus was 1.3 cm full width at half maximum (FWHM) horizontally and 0.6 cm FWHM vertically with a divergence of ±12 mrad. The mean momentum of the beam was determined by the final bending magnet with an accuracy of ±0.5%. The incident beam was counted in a three-counter telescope $S_1 S_2 S_3$ which defined the final spot size at the experimental target. Typically, with 6×10^{11} protons/pulse incident on the production target, the beam rate was 6×10^5 π^-/pulse.

The flux of leptons in the beam was determined by periodically moving a threshold Čerenkov counter into the beam. This counter was placed between $S1$ and $S2$ about 60 cm upstream of the hydrogen target, thus making any corrections due to the decay of beam particles negligible. The counter was verified to be 99.8% efficient. Electron and muon contaminations were measured at several momenta and a smooth handdrawn curve through the points was used to obtain final values for the lepton contamination. The total lepton contamination varied from (16 ± 2)% at 1.25 GeV/c to (1 ± 1)% at 3.0 GeV/c.

LIQUID HYDROGEN TARGET

The liquid hydrogen target used in the experiment was of the reservoir type. The target vessel itself was connected to a large reservoir which was filled with boiling liquid hydrogen at 1 atm pressure. The secondary cooling was provided by liquid nitrogen and the whole assembly was surrounded by a vacuum. The target vessel was a cylinder 5.08 cm in diameter and 10.68 cm long. The target vessel was made of 0.0076-cm Mylar wrapped with 13 layers of 0.00063-cm aluminized Mylar to provide thermal insulation. Both the beam particles and scattered particles saw a 0.051-cm window of the vacuum chamber. Provision was included to empty the target vessel.

The density of liquid hydrogen at 1-atm pressure and boiling temperature (20.3 °K) was 0.0708 g/cm^3. The number of protons per cm^2 was calculated to be $4.490 \times 10^{23} \pm 3\%$. The error is composed of ±2% uncertainty in the density of the liquid hydrogen and ±2% error in the length of the target vessel (taking into account the cylindrical shape of the vessel's ends, the beam profile, and possible fluctuations in a position of the center of the beam).

DETECTION APPARATUS

The experimental apparatus (Fig. 1) used to detect the final-state particles was an extension of that used in a previous experiment.[1] Recoil pions were detected in a 24-scintillation-counter array (A) which defined the scattering angle in the lab. This array was approximately 2.2 m from the target and covered the angular range from 177° to 67° in the laboratory. The horizontal size of these counters determined the resolution in $\cos\theta_{c.m.}$, ~±0.004 near 180° and ~±0.020 at wider angles. An additional counter (G) was required in fast coincidence in the trigger but did not define the geometrical acceptance. The pion arm kinematically determined the possible proton angular range from 0° to 20° in the lab. The magnet $M5$ selected positive particles in the forward direction such that the position of the scattered proton after $M5$ magnet was defined by two 16-element scintillation counter arrays (B) and (C). Each C counter was overmatched to the corresponding B counter so that only the B array defined the horizontal position of elastically scattered protons. This system provided a rough momentum cut of approximately 30% on the positive particles. This helped to reduce the inelastic background component in the trigger. The scintillation counter P, placed directly behind the B array, was the only counter which defined the vertical acceptance of the system. In addition, a system of veto counters (T) surrounded the target in regions outside the acceptance of the spectrometer. These counters were not part of the trigger system, but their status was recorded for each trigger. The event storage proceeded via several levels of logic in order to minimize dead times. An elastic trigger was generated by a fast coincidence between the beam $S_1S_2S_3$, a backward charged particle (G), and a forward positively charged particle (P). The trigger strobed the status of the latches of the A, B, and C arrays, as well as the target veto counters T. This trigger also generated a 55-μsec dead time in order to analyze the event. Each counter triggered during a 14-nsec gate was latched and sent to the event storage system. In addition, the time of flight between the A array and the C array was digitized and sent to the event storage system. Slow logic, applied to the latched signals before recording the event, required that only one element of the A array be present, and only one corresponding pair of elements from the B and C array be present. Finally, the time of flight was required to fall within a 9-nsec window. If all these conditions were met, the event was stored in the memory of a ND2200 analyzer. The 12-bit address of the analyzer was coded so that the four least significant bits gave the B-array counter number, bits 5 to 9 gave the A-array counter number, and bits 10 to 12 were used to record time-of-flight information and the status of the target veto counters. By mounting the phototubes for the A and C arrays at opposite ends of the scintillator, a degree of coplanarity was imposed on the detected events by the time-of-flight selection. The final timing resolution was taken as a full width at base of 6 nsec. Typically, the experiment generated fewer than 100 elastic triggers/pulse, of which 1–2/pulse satisfied the slow logic and were stored for the off-line analysis.

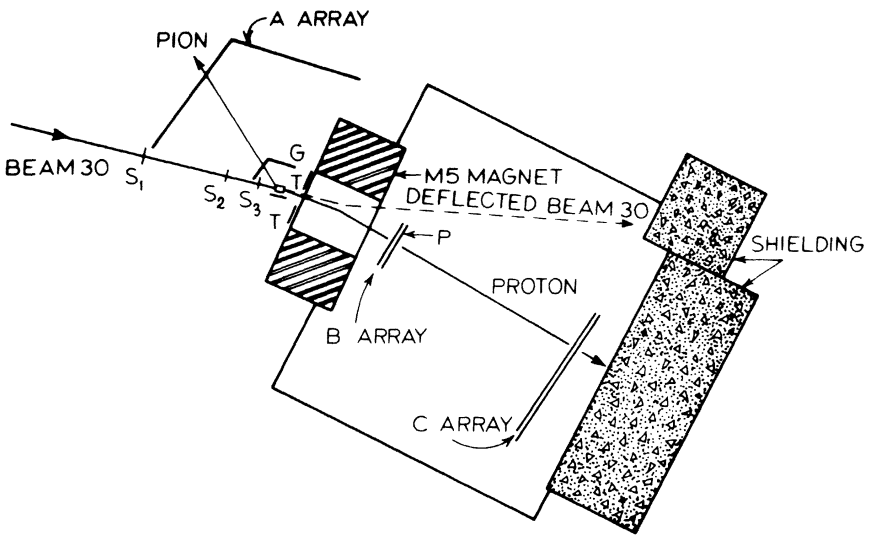

FIG. 1. Schematic plan view of the experimental layout.

DATA ANALYSIS

Data taking was divided into runs lasting several hours after which the analyzer memory was reproduced on paper tape and analyzed off-line in the CDC6600 computer. Target-empty runs were taken periodically at several momenta. Careful attention was paid to the effect of the instantaneous beam fluxes on various singles and coincidence rates because of the large RF duty factor during the experiment. The data were analyzed to obtain the differential cross sections $d\sigma/d\Omega_i$ $(1 \leq i \leq 24)$ defined by

$$\frac{d\sigma}{d\Omega_i} = C_i \frac{N_i^{\text{elastic}}}{N_\pi N_p \Delta\Omega_i},$$

where

N_i^{elastic} is the number of the "elastic events" detected in solid angle $\Delta\Omega_i$,

$\Delta\Omega_i$ is the solid angle in the center-of-mass system for the ith angular bin,

N_π is the number of incident pions detected by the beam telescope,

N_p is the number of protons per unit area in the liquid hydrogen target $[N_p = \rho L N_A / M_{H_2}$, ρ is the density of liquid hydrogen (g/cm^3), L is the length of the target flask (cm), N_A is Avogadro's number (mole^{-1}), and M_{H_2} is the atomic number of hydrogen (g/mole)],

C_i is the correction factor which takes into account the following:

(1) lepton contamination in the beam,
(2) nuclear absorption,
(3) pion decay,
(4) beam randoms,
(5) dead-time losses,
(6) counter inefficiencies,
(7) random loss of events due to A doubles.

In order to obtain the elastic events N_i^{elastic}, the stored events were plotted as a function of BC pairs for each A counter. Figure 2 shows a typical set of such distributions for a cross section of 10 μb/sr ($A16, \cos\theta_{\text{c.m.}} = -0.76$, $P^{\pi}_{\text{inc}} = 2.2$ GeV/c). The elastic angle–angle correlation is evident in these distributions. The number of events in the peak was determined by three methods: first, in the total spectrum, for which time-of-flight and target veto counter information is ignored, second, in the subtracted spectrum, the total sum spectrum minus the inelastic spectrum, and third, in the time-of-flight (TOF) spectrum, the sum of TOF bins which show elastic peaks. We demanded that all three methods produce the same answer to within 1 standard deviation. The widths and the position of the elastic peaks were calculated by using a Monte Carlo calculation. The number of events in the peak was determined by drawing a

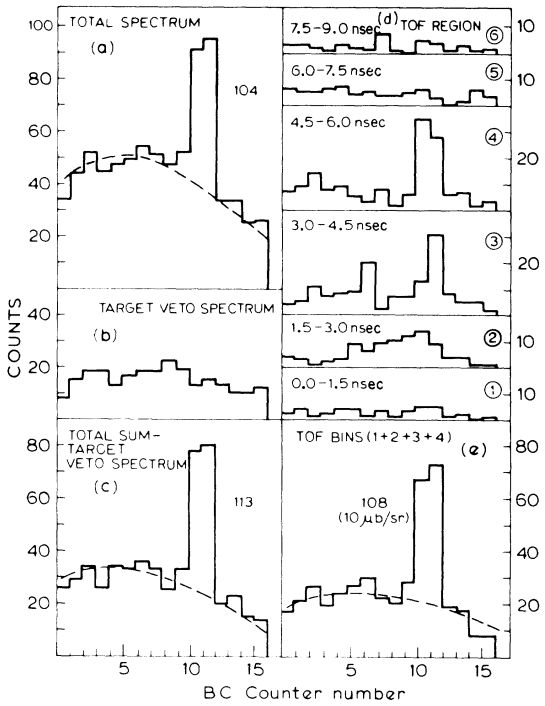

FIG. 2. Number of events in each BC pair of counters for a single A counter for (a) the total spectrum; (b) the spectrum associated with T counter triggers; (c) spectrum (a) – spectrum (b); (d) six regions of time-of-flight between the A counter and C counter; (e) the sum of four time-of-flight bins 1, 2, 3, 4.

smooth background for each spectrum and subtracting the background events from the peak events. Finally, to obtain N_i^{elastic}, the target-empty elastic contribution was subtracted. The target-empty contribution was determined separately using the target-empty total sum spectrum in a similar manner to the target-full spectra. Because of reduced statistics for these runs, the number of target-empty events was determined for each A counter at a given momentum and smoothed as a function of angle (Fig. 3). Finally, the numbers thus obtained were smoothed as a function of momentum for each A counter. Percentage errors were determined from raw data and similarly smoothed. These errors varied from 30 to 80% and they increased the overall statistical error by less than 1%. The total subtraction necessary varied between 5 and 35%, of which about 30% was due to target-empty events. The shapes of the inelastic spectra generated using the Monte Carlo program FOWL[2] events showed a smooth contribution in the elastic region. The statistical error was determined by adding in quadrature the statistical errors in the number of elastic events, background events, and target-

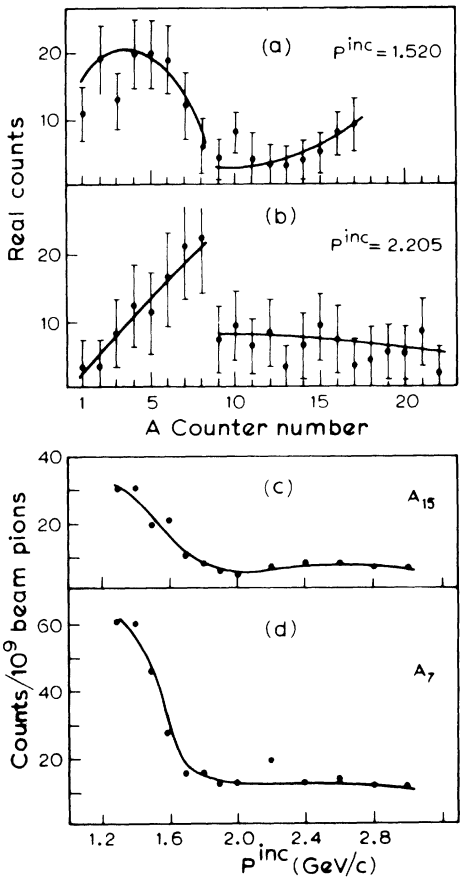

FIG. 3. Target-empty contribution as a function of (a) A counter at 1.52 GeV/c; (b) A counter at 2.205 GeV/c; (c) incident pion momentum for counter A_{15}; (d) incident pion momentum for counter A_7. The lines are the smoothed functions used in the data analysis.

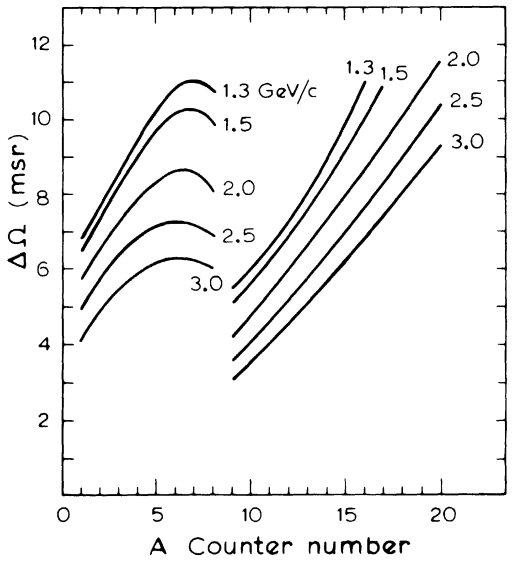

FIG. 4. Monte Carlo calculations of the experimental acceptance, at 5 incident pion momenta, as a function of A counter.

empty events. This error was ±6% for a 50-μb/sr cross section.

Solid angles were generated by a Monte Carlo program, which simulated the πp elastic scattering (Fig. 4). In this simulation it was required that the pion hit the G and A counters, and the proton, after bending in the magnet, hit the P counter and the appropriate BC pair. In addition, the following effects were taken into account. The beam momentum was uniformly randomized within the momentum bite. The target size placed a constraint on possible interaction origins, and was populated uniformly in the longitudinal direction of the target and according to a Gaussian shape in the vertical and horizontal directions of the target. The incident beam direction was uniformly generated within limits given by the S_1 counter and the interaction region in the target. The multiple Coulomb scattering of the final-state particles was calculated in the liquid hydrogen, the target walls, the air, the scintillators and their wrappings. Deflection angles due to multiple scattering in each material were generated according to a Gaussian shape, with the standard deviation equal to the root-mean-square scattering angle for the material. Energy loss of the scattered particles was not considered in the calculation because its effect was negligible. The solid angles were generated at incident momenta of 1.3, 1.5, 2.0, 2.5, and 3.0 GeV/c, and then fitted with a low-order polynomial as a function of angle and momentum to get values at any intermediate momentum. The fitted errors were typically between 2–4%. The typical values of the solid angles were of the order of 3–12 msr. The focusing effect of the $M5$ target, which tends to increase the solid angles, was estimated to be less than 1%.

CORRECTIONS TO THE DATA

Several other correction factors which have been applied to the data are shown in Table I, along with the uncertainty associated with each factor.

Nuclear absorption of the incident beam and scattered particles were determined by hand calculations using total-cross-section data. Pion decays were estimated using a Monte Carlo simulation. Beam counting losses due to rf structure present during the experiment varied up to 10% at the higher momenta where large fluxes were required. The rf structure was measured using delayed coincidences and confirmed independently to be 20%. This figure was used to calculate the beam losses. Losses also occur in counting the recoil pions since we demanded only one recoil

TABLE I. Correction factors and individual contributions to the overall systematic error on the differential cross sections.

Correction	Factor	Error
Lepton contamination	(1.01–1.19)	±2%
Absorption of the beam	1.01	±1%
Absorption of the scattered particles	(1.07–1.09)	±2%
Pion decay	1.00	±1%
rf-structure losses	(0.89–0.96)	±3%
A doubles	1.025	±1%
Beam randoms	1.01	±1%
Counter inefficiencies and gaps in the arrays	1.015	±0%
Other systematic uncertainties:		
Solid angles		±(2–4)%
Number of target protons		±3%
Total correction and overall uncertainties	(1.03–1.35)	±(6–7)%

counter to be present. These losses amount to 2.5%. The overall systematic correction varied from 3 to 35% and contributes a systematic error of 6–7% in the normalization.

DISCUSSION OF THE DATA

The data cover a center-of-mass angular region of 125°–178° and a momentum interval from 1.28 to 3.0 GeV/c. The differential cross section varies typically between 500 μb/sr at 1.28 GeV/c and 20 μb/sr at 3.0 GeV/c; however, in the dip regions it goes as low as 1–2 μb/sr. In the following we describe the main features of the data.

In the momentum region between 1.28 and 1.5 GeV/c the $\pi^- p$ differential cross section is relatively structureless. This can be seen in Fig. 5. The main feature is a change of a slope of the cross section at 180°. Near 1.3 GeV/c the cross section decreases as the angle approaches 180°, around 1.4 GeV/c the cross section flattens, and as one goes up to 1.5 GeV/c the cross section rises as the angle approaches 180°. The error bars are statistical only (typically ±5%).

The most interesting features of the data occur above 1.5 GeV/c. A narrow dip appears in the differential cross section at angles from 130° to 150° in the center-of-mass frame, and a turnover at 180° appears near 2.1 GeV/c. This can be seen in Fig. 6 in which we show some representative differential cross sections distributed over the range of pion momenta 1.5–3.0 GeV/c. The beginning of the dip is at an incident momentum of 1.5 GeV/c, and as one goes up in energy the depth of the dip increases until the pion momentum reaches 2.1 GeV/c. Above this momentum the dip becomes broader and at 3.0 GeV/c it is not evident in the data. In all cases where the dip is seen we have at least five data points to determine its shape. The turnover near 180°, i.e., the rapid decrease in cross sections near 180°, extends over an interval of p^{inc} of 0.2 GeV/c centered at 2.1 GeV/c. One should stress that within the angular range of $-0.96 < \cos\theta_{\text{c.m.}} < -1.0$ the cross section changes its value by a factor of ~10. We have from 4 to 6 data points at each momentum to see this change. Somewhere around 2.6 GeV/c the turnover flattens out and near 3.0 GeV/c we see the onset of a backward peak. The error bars indicated are statistical only and are typically ±6% for a differential cross section of 50 μb/sr. In a previous publication[3] we have discussed the position of the dip at different incident momenta. We have concluded that the occurrence of the dip in the cross section and the rapid fall in this 180° cross section are closely related to the interference of high-spin resonant amplitudes at this πp mass. We will discuss this in more detail in a later publication.

Figure 7 shows a comparison of this experiment with other data. The graphs compare our data with the data of Crabb *et al.*[1] (our previous experiment) and Rothschild *et al.*[4] at 1.28 GeV/c, and the data of Carroll *et al.*[5] and Kormanyos *et al.*[6] at 2.3-GeV/c incident momentum. Generally we can say

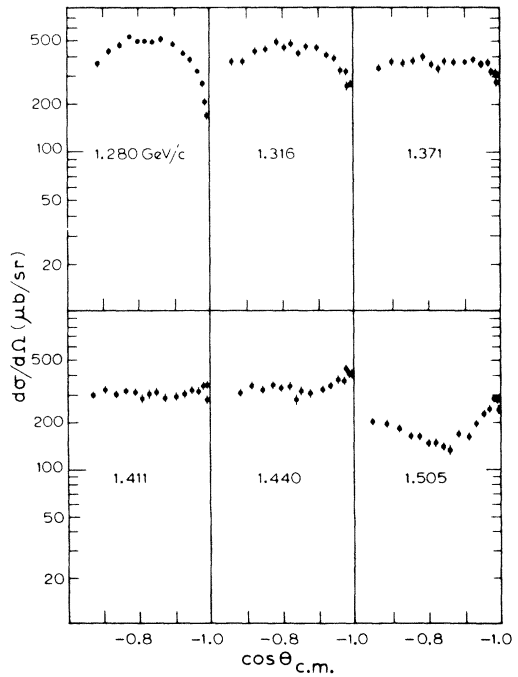

FIG. 5. Differential cross sections from 1.28 to 1.505 GeV/c.

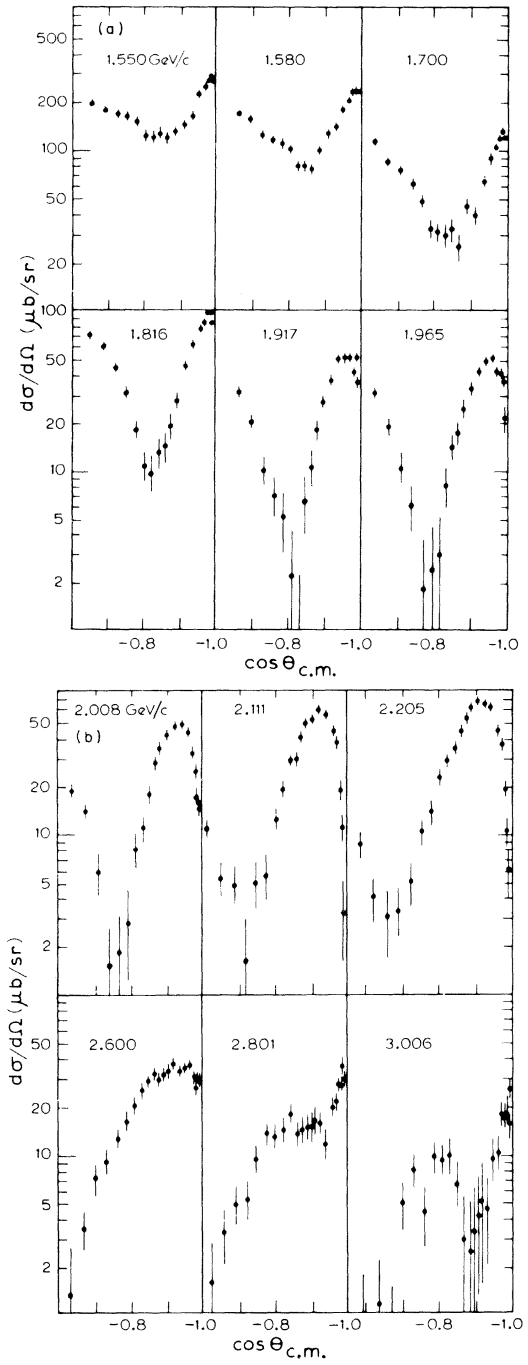

FIG. 6. Differential cross sections from (a) 1.55 to 1.965 GeV/c, and (b) 2.008 to 3.006 GeV/c.

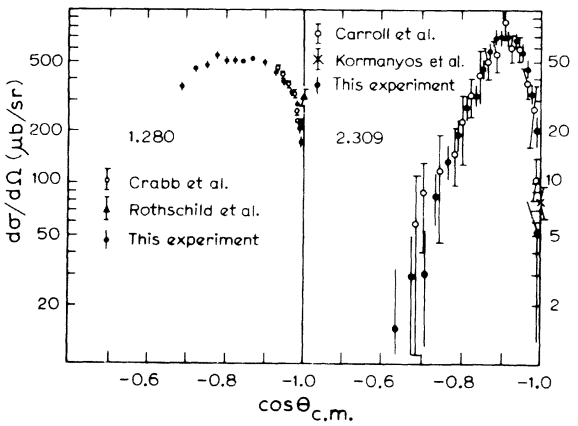

FIG. 7. Comparison of our data with (a) the data of Crabb *et al.* and Rothschild *et al.* at 1.28 GeV/c, and (b) the data of Carroll *et al.* and Kormanyos *et al.* at 2.309 GeV/c.

that there is an agreement between this experiment and most of the other data, including the data of Crittenden *et al.*[7] and Aplin *et al.*[8]. However, at several momenta we disagree with the results of Abillon *et al.*[9] and Rothschild *et al.*[4]. Table II lists all our data as a function of momentum and angle.

In Fig. 8 we compare our data with the latest phase-shift solution of Ayed *et al.* (SACLAY 74).[10] This solution is able to follow the general trends of the data and can reproduce the rapid change of cross section in the momentum region near 2.0 GeV/c. Also, the predictions at higher momenta are in excellent agreement with our data. It is surprising that it is in the momentum region below

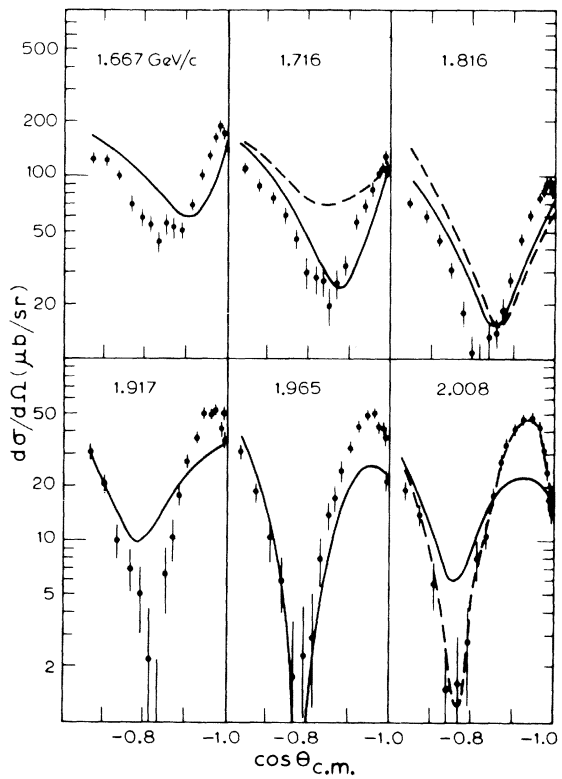

FIG. 8. Comparison of our data with the predictions of the SACLAY 74 phase-shift analysis at 6 momenta.

TABLE II. Differential cross sections as a function of beam momentum and center-of-mass scattering angle. The errors are purely statistical.

P_{beam} (GeV/c)	$\cos\theta_{c.m.}$	$\frac{d\sigma}{d\Omega}$ (μb/sr)	P_{beam} (GeV/c)	$\cos\theta_{c.m.}$	$\frac{d\sigma}{d\Omega}$ (μb/sr)
1.280	−0.9986	172 ± 14	1.293	−0.9986	210 ± 17
	−0.9939	207 ± 14		−0.9940	261 ± 18
	−0.9851	275 ± 15		−0.9852	237 ± 16
	−0.9715	323 ± 16		−0.9717	326 ± 18
	−0.9529	384 ± 16		−0.9532	366 ± 18
	−0.9293	437 ± 17		−0.9298	405 ± 18
	−0.9014	484 ± 17		−0.9021	474 ± 20
	−0.8705	520 ± 18		−0.8714	483 ± 21
	−0.8453	500 ± 26		−0.8463	512 ± 29
	−0.8267	503 ± 24		−0.8278	477 ± 27
	−0.8056	502 ± 23		−0.8069	492 ± 26
	−0.7818	548 ± 22		−0.7832	479 ± 24
	−0.7551	474 ± 19		−0.7567	453 ± 22
	−0.7254	447 ± 18		−0.7271	461 ± 21
	−0.6926	365 ± 16		−0.6945	424 ± 19
				−0.6588	344 ± 16
1.316	−0.9986	265 ± 19	1.360	−0.9986	245 ± 15
	−0.9940	261 ± 17		−0.9943	296 ± 16
	−0.9854	319 ± 18		−0.9857	268 ± 15
	−0.9721	326 ± 18		−0.9727	323 ± 16
	−0.9538	392 ± 19		−0.9549	298 ± 15
	−0.9307	409 ± 19		−0.9323	341 ± 15
	−0.9033	456 ± 19		−0.9055	341 ± 15
	−0.8729	464 ± 20		−0.8757	370 ± 16
	−0.8481	416 ± 27		−0.8515	350 ± 22
	−0.8298	487 ± 27		−0.8335	352 ± 20
	−0.8091	459 ± 25		−0.8132	369 ± 20
	−0.7857	495 ± 25		−0.7902	347 ± 18
	−0.7594	448 ± 22		−0.7644	331 ± 18
	−0.7301	438 ± 21		−0.7356	303 ± 16
	−0.6978	375 ± 18		−0.7039	296 ± 14
	−0.6624	376 ± 17		−0.6691	276 ± 13
1.371	−0.9986	283 ± 19	1.390	−0.9987	264 ± 18
	−0.9942	323 ± 19		−0.9943	288 ± 18
	−0.9858	330 ± 18		−0.9860	299 ± 17
	−0.9729	371 ± 19		−0.9732	308 ± 18
	−0.9551	363 ± 18		−0.9556	337 ± 17
	−0.9326	389 ± 18		−0.9333	307 ± 16
	−0.9060	372 ± 18		−0.9069	309 ± 16
	−0.8764	377 ± 19		−0.8776	340 ± 17
	−0.8523	381 ± 26		−0.8537	320 ± 23
	−0.8344	342 ± 24		−0.8360	311 ± 22
	−0.8142	367 ± 23		−0.8159	325 ± 21
	−0.7913	409 ± 22		−0.7932	342 ± 20
	−0.7656	377 ± 21		−0.7677	324 ± 19
	−0.7370	364 ± 19		−0.7393	309 ± 17
	−0.7054	378 ± 18		−0.7080	306 ± 16
	−0.6707	340 ± 17		−0.6735	243 ± 14
1.411	−0.9987	276 ± 19	1.440	−0.9987	400 ± 22
	−0.9943	346 ± 20		−0.9944	406 ± 21
	−0.9861	345 ± 18		−0.9863	441 ± 21
	−0.9735	315 ± 18		−0.9739	368 ± 20
	−0.9561	323 ± 17		−0.9567	364 ± 19
	−0.9340	301 ± 16		−0.9350	334 ± 17

TABLE II. (*Continued*)

P_{beam} (GeV/c)	$\cos\theta_{c.m.}$	$\frac{d\sigma}{d\Omega}$ (μb/sr)	P_{beam} (GeV/c)	$\cos\theta_{c.m.}$	$\frac{d\sigma}{d\Omega}$ (μb/sr)
1.411	−0.9079	291 ± 16	1.440	−0.9092	321 ± 18
	−0.8789	279 ± 16		−0.8806	301 ± 17
	−0.8551	311 ± 23		−0.8572	316 ± 25
	−0.8376	305 ± 22		−0.8399	269 ± 21
	−0.8178	278 ± 20		−0.8202	330 ± 21
	−0.7953	310 ± 20		−0.7980	327 ± 20
	−0.7700	318 ± 19		−0.7731	334 ± 20
	−0.7418	306 ± 17		−0.7452	316 ± 18
	−0.7107	321 ± 17		−0.7144	339 ± 17
	−0.6765	292 ± 15		−0.6806	301 ± 16
1.480	−0.9987	256 ± 17	1.505	−0.9987	239 ± 12
	−0.9945	272 ± 16		−0.9946	281 ± 12
	−0.9866	282 ± 15		−0.9868	280 ± 11
	−0.9744	262 ± 15		−0.9745	245 ± 11
	−0.9576	224 ± 13		−0.9581	224 ± 10
	−0.9362	195 ± 12		−0.9370	195 ± 9
	−0.9110	171 ± 11		−0.9120	162 ± 8
	−0.8829	167 ± 12		−0.8842	167 ± 8
	−0.8599	172 ± 16		−0.8615	135 ± 10
	−0.8428	152 ± 15		−0.8447	140 ± 10
	−0.8236	167 ± 14		−0.8256	144 ± 10
	−0.8017	202 ± 15		−0.8040	144 ± 9
	−0.7771	208 ± 14		−0.7796	162 ± 9
	−0.7497	217 ± 13		−0.7524	162 ± 9
	−0.7194	199 ± 12		−0.7224	183 ± 8
	−0.6860	178 ± 12		−0.6893	192 ± 8
	−0.6493	220 ± 11		−0.6529	196 ± 8
1.523	−0.9987	272 ± 16	1.550	−0.9988	280 ± 15
	−0.9946	318 ± 16		−0.9947	293 ± 14
	−0.9869	277 ± 14		−0.9871	279 ± 13
	−0.9749	233 ± 13		−0.9752	255 ± 12
	−0.9585	220 ± 12		−0.9590	229 ± 12
	−0.9376	173 ± 11		−0.9384	163 ± 10
	−0.9128	167 ± 11		−0.9139	148 ± 9
	−0.8852	155 ± 10		−0.8866	131 ± 9
	−0.8626	120 ± 13		−0.8643	119 ± 12
	−0.8459	136 ± 13		−0.8478	130 ± 12
	−0.8270	132 ± 12		−0.8291	123 ± 11
	−0.8055	158 ± 12		−0.8079	124 ± 11
	−0.7814	160 ± 12		−0.7839	157 ± 10
	−0.7543	190 ± 12		−0.7572	167 ± 10
	−0.7245	190 ± 11		−0.7277	172 ± 10
	−0.6917	199 ± 11		−0.6951	180 ± 9
	−0.6554	222 ± 11		−0.6592	204 ± 9
1.580	−0.9988	245 ± 12	1.590	−0.9988	256 ± 13
	−0.9948	236 ± 11		−0.9948	269 ± 13
	−0.9872	236 ± 10		−0.9873	258 ± 12
	−0.9756	206 ± 10		−0.9757	222 ± 11
	−0.9596	177 ± 9		−0.9598	180 ± 10
	−0.9392	140 ± 8		−0.9395	155 ± 9
	−0.9151	127 ± 7		−0.9155	138 ± 8
	−0.8882	98 ± 7		−0.8887	105 ± 8
	−0.8861	77 ± 8		−0.8668	71 ± 9
	−0.8498	80 ± 8		−0.8505	84 ± 9

TABLE II. (*Continued*)

P_{beam} (GeV/c)	$\cos\theta_{c.m.}$	$\frac{d\sigma}{d\Omega}$ (μb/sr)	P_{beam} (GeV/c)	$\cos\theta_{c.m.}$	$\frac{d\sigma}{d\Omega}$ (μb/sr)
1.580	−0.8314	78 ± 7	1.590	−0.8321	96 ± 9
	−0.8104	104 ± 8		−0.8112	109 ± 9
	−0.7867	111 ± 7		−0.7877	119 ± 9
	−0.7603	118 ± 7		−0.7613	129 ± 9
	−0.7311	124 ± 7		−0.7322	142 ± 8
	−0.6989	160 ± 8		−0.7001	187 ± 9
	−0.6633	171 ± 7		−0.6647	179 ± 8
1.667	−0.9988	179 ± 10	1.700	−0.9988	127 ± 9
	−0.9950	175 ± 10		−0.9951	134 ± 8
	−0.9878	190 ± 9		−0.9879	121 ± 8
	−0.9766	164 ± 8		−0.9769	106 ± 7
	−0.9612	129 ± 7		−0.9617	86 ± 6
	−0.9416	102 ± 6		−0.9424	66 ± 6
	−0.9184	72 ± 6		−0.9195	39 ± 5
	−0.8924	51 ± 5		−0.8940	46 ± 5
	−0.8712	52 ± 7		−0.8730	25 ± 5
	−0.8555	54 ± 7		−0.8575	32 ± 6
	−0.8376	45 ± 6		−0.8398	29 ± 5
	−0.8173	54 ± 6		−0.8198	32 ± 5
	−0.7944	60 ± 6		−0.7972	33 ± 5
	−0.7688	72 ± 6		−0.7719	48 ± 5
	−0.7405	102 ± 7		−0.7439	62 ± 5
	−0.7092	122 ± 7		−0.7130	75 ± 5
	−0.6747	124 ± 6		−0.6788	84 ± 5
				−0.6420	113 ± 6
1.716	−0.9989	113 ± 8	1.768	−0.9989	118 ± 7
	−0.9951	131 ± 8		−0.9952	122 ± 7
	−0.9880	113 ± 7		−0.9883	108 ± 7
	−0.9771	106 ± 7		−0.9776	109 ± 6
	−0.9620	85 ± 7		−0.9629	86 ± 6
	−0.9429	69 ± 6		−0.9441	56 ± 5
	−0.9201	57 ± 5		−0.9219	52 ± 5
	−0.8947	33 ± 5		−0.8970	28 ± 4
	−0.8739	26 ± 5		−0.8766	19 ± 5
	−0.8584	20 ± 5		−0.8615	14 ± 5
	−0.8409	27 ± 5		−0.8443	12 ± 4
	−0.8210	28 ± 5		−0.8248	13 ± 4
	−0.7985	31 ± 5		−0.8027	24 ± 4
	−0.7734	46 ± 5		−0.7780	33 ± 4
	−0.7455	62 ± 5		−0.7507	53 ± 5
	−0.7148	77 ± 5		−0.7204	66 ± 5
	−0.6807	92 ± 6		−0.6869	84 ± 5
	−0.6441	110 ± 6		−0.6509	95 ± 5
1.816	−0.9989	84 ± 5	1.865	−0.9989	67 ± 4
	−0.9953	99 ± 5		−0.9954	76 ± 4
	−0.9885	99 ± 5		−0.9888	75 ± 4
	−0.9781	86 ± 4		−0.9785	74 ± 4
	−0.9636	78 ± 4		−0.9644	61 ± 3
	−0.9453	62 ± 4		−0.9464	54 ± 3
	−0.9234	47 ± 3		−0.9250	40 ± 3
	−0.8990	28 ± 3		−0.9010	26 ± 3
	−0.8790	19 ± 3		−0.8814	17 ± 3
	−0.8642	14 ± 3		−0.8668	8.8 ± 3
	−0.8473	13 ± 3		−0.8502	6.7 ± 3
	−0.8281	10 ± 3		−0.8314	7.4 ± 2

TABLE II. (*Continued*)

P_{beam} (GeV/c)	$\cos\theta_{c.m.}$	$\frac{d\sigma}{d\Omega}$ (μb/sr)	P_{beam} (GeV/c)	$\cos\theta_{c.m.}$	$\frac{d\sigma}{d\Omega}$ (μb/sr)
1.816	−0.8064	11 ± 3	1.865	−0.8101	8.5 ± 2
	−0.7821	18 ± 3		−0.7862	12 ± 2
	−0.7552	32 ± 3		−0.7597	20 ± 2
	−0.7254	45 ± 3		−0.7304	28 ± 2
	−0.6924	62 ± 3		−0.6979	40 ± 3
	−0.6569	72 ± 3		−0.6628	56 ± 3
1.917	−0.9990	36 ± 3	1.965	−0.9990	21 ± 3
	−0.9955	52 ± 4		−0.9956	37 ± 3
	−0.9890	41 ± 4		−0.9892	42 ± 3
	−0.9790	52 ± 3		−0.9794	43 ± 3
	−0.9651	50 ± 3		−0.9658	51 ± 3
	−0.9475	51 ± 3		−0.9485	49 ± 3
	−0.9265	38 ± 3		−0.9279	43 ± 3
	−0.9031	27 ± 3		−0.9049	34 ± 3
	−0.8838	18 ± 3		−0.8859	25 ± 3
	−0.8695	11 ± 3		−0.8719	17 ± 3
	−0.8532	6.5 ± 3		−0.8559	14 ± 3
	−0.8347	0.3 ± 2		−0.8377	8.2 ± 2
	−0.8138	2.2 ± 2		−0.8171	3.0 ± 2
	−0.7903	5.1 ± 2		−0.7940	2.4 ± 2
	−0.7643	7.0 ± 2		−0.7684	1.8 ± 2
	−0.7354	10 ± 2		−0.7399	6.0 ± 2
	−0.7034	21 ± 2		−0.7084	11 ± 2
	−0.6689	32 ± 2		−0.6743	19 ± 2
				−0.6381	31 ± 2
2.008	−0.9990	15 ± 2	2.111	−0.9990	3.3 ± 1.8
	−0.9957	17 ± 3		−0.9958	11 ± 2
	−0.9894	24 ± 3		−0.9898	19 ± 3
	−0.9797	33 ± 3		−0.9805	37 ± 3
	−0.9664	44 ± 3		−0.9677	45 ± 3
	−0.9494	48 ± 3		−0.9513	56 ± 3
	−0.9291	48 ± 3		−0.9318	62 ± 3
	−0.9064	41 ± 3		−0.9100	53 ± 3
	−0.8878	34 ± 4		−0.8920	49 ± 4
	−0.8739	28 ± 3		−0.8786	41 ± 4
	−0.8582	18 ± 2		−0.8634	30 ± 3
	−0.8402	11 ± 2		−0.8461	29 ± 3
	−0.8200	8.1 ± 2		−0.8265	19 ± 2
	−0.7972	2.7 ± 2		−0.8044	12 ± 2
	−0.7719	1.6 ± 1		−0.7799	5.6 ± 1.8
	−0.7438	1.5 ± 1		−0.7527	4.9 ± 1.6
	−0.7127	5.7 ± 2		−0.7225	1.6 ± 1.3
	−0.6790	14 ± 2		−0.6897	4.9 ± 1.3
	−0.6432	19 ± 2		−0.6549	5.2 ± 1.3
				−0.6163	11 ± 1.6
2.205	−0.9991	6.1 ± 2.0	2.309	−0.9991	5.1 ± 3.7
	−0.9960	11 ± 2		−0.9961	11 ± 4
	−0.9902	20 ± 3		−0.9906	20 ± 4
	−0.9812	37 ± 3		−0.9819	33 ± 5
	−0.9688	45 ± 3		−0.9699	45 ± 5
	−0.9530	63 ± 3		−0.9547	58 ± 6
	−0.9341	66 ± 3		−0.9365	68 ± 6
	−0.9130	67 ± 4		−0.9161	69 ± 6
	−0.8956	62 ± 5		−0.8992	69 ± 8
	−0.8826	52 ± 4		−0.8867	69 ± 7

TABLE II. (*Continued*)

P_{beam} (GeV/c)	$\cos\theta_{c.m.}$	$\frac{d\sigma}{d\Omega}$ (μb/sr)	P_{beam} (GeV/c)	$\cos\theta_{c.m.}$	$\frac{d\sigma}{d\Omega}$ (μb/sr)
2.205	−0.8679	44 ± 4	2.309	−0.8725	57 ± 7
	−0.8511	35 ± 3		−0.8562	44 ± 5
	−0.8320	29 ± 3		−0.8378	32 ± 5
	−0.8106	23 ± 2		−0.8170	27 ± 4
	−0.7868	13 ± 2		−0.7939	19 ± 4
	−0.7603	10 ± 2		−0.7682	13 ± 3
	−0.7309	4.9 ± 1.6		−0.7396	8.4 ± 2.8
	−0.6990	3.3 ± 1.2		−0.7085	3.0 ± 1.9
	−0.6649	3.0 ± 1.4		−0.6754	2.8 ± 2.2
	−0.6272	3.9 ± 1.2		−0.6385	1.4 ± 1.9
	−0.5876	8.4 ± 1.5			
2.412	−0.9991	18 ± 3	2.515	−0.9992	23 ± 3
	−0.9963	18 ± 3		−0.9964	27 ± 3
	−0.9909	24 ± 3		−0.9912	28 ± 3
	−0.9825	37 ± 3		−0.9831	32 ± 3
	−0.9710	43 ± 4		−0.9720	42 ± 3
	−0.9563	59 ± 4		−0.9577	45 ± 3
	−0.9387	61 ± 4		−0.9407	47 ± 3
	−0.9189	69 ± 4		−0.9216	48 ± 3
	−0.9027	54 ± 5		−0.9058	44 ± 4
	−0.8905	55 ± 5		−0.8941	42 ± 4
	−0.8767	48 ± 4		−0.8807	39 ± 3
	−0.8610	42 ± 4		−0.8654	41 ± 3
	−0.8431	39 ± 3		−0.8480	32 ± 3
	−0.8229	32 ± 3		−0.8285	32 ± 3
	−0.8005	23 ± 3		−0.8067	23 ± 2
	−0.7755	20 ± 2		−0.7824	15 ± 2
	−0.7476	9.1 ± 1.8		−0.7552	16 ± 2
	−0.7174	4.6 ± 1.6		−0.7258	6.8 ± 1.5
	−0.6851	5.0 ± 1.4		−0.6942	4.1 ± 1.4
	−0.6491	2.8 ± 1.2		−0.6591	2.2 ± 1.2
	−0.6113	3.2 ± 1.3		−0.6221	3.1 ± 1.2
	−0.5719	5.5 ± 1.2		−0.5835	3.9 ± 1.1
2.600	−0.9992	29 ± 3	2.801	−0.9992	29 ± 3
	−0.9965	29 ± 3		−0.9967	36 ± 3
	−0.9914	25 ± 3		−0.9920	27 ± 3
	−0.9836	30 ± 3		−0.9846	27 ± 3
	−0.9727	37 ± 3		−0.9744	21 ± 3
	−0.9589	35 ± 3		−0.9613	19 ± 3
	−0.9423	33 ± 3		−0.9457	11 ± 3
	−0.9237	38 ± 3		−0.9282	15 ± 3
	−0.9083	33 ± 4		−0.9137	16 ± 3
	−0.8968	32 ± 3		−0.9028	15 ± 3
	−0.8838	29 ± 3		−0.8905	14 ± 3
	−0.8689	32 ± 3		−0.8764	14 ± 3
	−0.8519	29 ± 3		−0.8603	13 ± 2
	−0.8328	25 ± 3		−0.8422	18 ± 2
	−0.8115	21 ± 2		−0.8220	14 ± 2
	−0.7877	16 ± 2		−0.7994	13 ± 2
	−0.7612	12 ± 2		−0.7741	13 ± 2
	−0.7323	8.9 ± 1.6		−0.7466	9.4 ± 1.7
	−0.7014	7.0 ± 1.5		−0.7171	5.1 ± 1.5
	−0.6669	3.5 ± 1.4		−0.6841	4.8 ± 1.4
	−0.6306	1.3 ± 1.3		−0.6492	3.3 ± 1.3
	−0.5926	1.0 ± 1.0		−0.6127	1.6 ± 1.2
				−0.5739	2.1 ± 1.2

TABLE II. (*Continued*)

P_{beam} (GeV/c)	$\cos\theta_{c.m.}$	$\frac{d\sigma}{d\Omega}$ (μb/sr)
3.006	−0.9993	26 ± 3
	−0.9969	16 ± 4
	−0.9924	20 ± 3
	−0.9855	18 ± 3
	−0.9759	18 ± 3
	−0.9636	10 ± 3
	−0.9488	9.5 ± 2.9
	−0.9323	4.7 ± 2.7
	−0.9185	5.3 ± 3.5
	−0.9083	4.3 ± 2.9
	−0.8966	3.4 ± 2.8
	−0.8832	2.5 ± 2.6
	−0.8680	3.0 ± 2.5
	−0.8508	6.6 ± 1.9
	−0.8315	10 ± 3.0
	−0.8100	9.4 ± 2.2
	−0.7860	9.7 ± 2.1
	−0.7597	4.5 ± 1.9
	−0.7314	8.0 ± 1.8
	−0.6998	4.9 ± 1.6
	−0.6664	0.2 ± 1.5
	−0.6312	1.1 ± 1.2
	−0.5938	0.6 ± 1.3

1.9 GeV/c that the predictions disagree most with the data. An examination of the baryon table in the latest Particle Data Group listings[11] shows that most of the resonances in this momentum region fall into the one- and two-star category, with the exception of the $\Delta(1910)$ $P31$ and $\Delta(1950)$ $F37$ resonances. This may explain the disagreement between the phase-shift predictions and the cross-section data. The existing $\pi^- p$ elastic polarization data in this momentum region is of very poor quality, especially at backward angles. It is therefore expected that our measurements of the cross section in this region may give further useful information on the resonant structure in the $\pi^- p$ mass region of 1.9–2.1 GeV. Clearly also better measurements of the polarization parameter in this mass and angular region are necessary.

In a subsequent publication we will compare our data with a multiresonance direct-channel fit, which will give predictions for the expected polarization angular distribution and may also add information about the resonance parameters in the momentum region below 2.5 GeV/c.

CONCLUSIONS

We have measured the backward differential cross section in $\pi^- p$ elastic scattering at 31 momenta from 1.28 to 3.0 GeV/c. The data cover the pion center-of-mass scattering angle in the region $-0.570 \leq \cos\theta_{c.m.} \leq -0.999$. We have compared these data with data from other experiments and the predictions of the latest phase-shift solution. There is good agreement with other data in the regions of overlap. The phase-shift predictions are in excellent agreement with the data in the momentum region above 1.9 GeV/c but below this momentum the agreement is not good. We surmise that this is due to the imprecise measurements of the parameters of several weakly confirmed baryon states in the mass region 1.9–2.1 GeV.

ACKNOWLEDGMENTS

We wish to thank the Bevatron staff, and in particular Dr. R. Sah, for their assistance during the course of this work.

*Present address: Carleton University, Ottawa, Ontario, Canada.
†Present address: Rutherford Laboratory, Chilton, Didcot, Oxon OX11 OQX, England.
‡Present address: Research Department, Caterpillar Tractor Company, Peoria, Illinois 61602.
§Present address: Lawrence Berkeley Laboratory, Berkeley, California 94720.

[1]D. G. Crabb, R. Keller, J. R. O'Fallon, T. J. Richards, R. J. Ott, J. M. Trischuk, J. Va'Vra, and L. S. Schroeder, Phys. Rev. Lett. 27, 216 (1971).
[2]F. James, CERN report (unpublished).
[3]R. J. Ott, J. M. Trischuk, J. Va'Vra, T. J. Richards, and L. S. Schroeder, Phys. Lett. 42B, 133 (1972).
[4]R. E. Rothschild, T. Bowen, P. D. Caldwell, D. Davidson, E. W. Jenkins, R. M. Kalbach, D. V. Petersen, and A. E. Pifer, Phys. Rev. D 5, 499 (1972).
[5]A. S. Carroll, J. Fischer, A. Lundby, R. H. Phillips, C. L. Wang, F. Lobkowicz, A. C. Melissinos, Y. Nagashima, and S. Tewksbury, Phys. Rev. Lett. 20, 607 (1968).
[6]S. W. Kormanyos, A. D. Krisch, J. R. O'Fallon, K. Ruddick, and L. Ratner, Phys. Rev. Lett. 16, 709 (1966).
[7]R. R. Crittenden, K. F. Galloway, R. M. Heinz, H. A. Neal, and R. A. Sidwell, Phys. Rev. D 1, 3050 (1970).
[8]P. S. Aplin, I. M. Cowan, W. M. Gibson, R. S. Gilmore, K. Green, J. Malos, V. J. Smith, D. L. Ward, M. A. R. Kemp, A. T. Lea, R. McKenzie, and G. C. Oades, Nucl. Phys. B32, 253 (1971).
[9]J. M. Abillon, A. Borg, M. Crozon, T. Leray, J. P. Mendiburu, and J. Tocqueville, Phys. Lett. 32B, 712 (1970).
[10]R. Ayed, P. Bareyre, and Y. Lemoigne, CEN-Saclay report, 1972 (unpublished).
[11]Particle Data Group, Rev. Mod. Phys. 48, S1 (1976).